Journal of Electron Spectroscopy and Related Phenomena 213 (2016) 17–21

Contents lists available at ScienceDirect

Journal of Electron Spectroscopy and Related Phenomena

journal homepage: www.elsevier.com/locate/elspec

Electron emission relevant to inner-shell photoionization of condensed water studied by multi-electron coincidence spectroscopy

Y. Hikosaka[a,*], R. Mashiko[b], Y. Konosu[b], K. Soejima[b], E. Shigemasa[c,d]

[a] Graduate School of Medicine and Pharmaceutical Sciences, University of Toyama, Toyama 930-0194, Japan
[b] Department of Environmental Science, Niigata University, Niigata 950-2181, Japan
[c] UVSOR Facility, Institute for Molecular Science, Okazaki 444-8585, Japan
[d] SOKENDAI, Okazaki 444-8585, Japan

ARTICLE INFO

Article history:
Received 4 September 2016
Received in revised form 17 October 2016
Accepted 18 October 2016
Available online 5 November 2016

Keywords:
Condensed water
Auger decay
Multi-electron coincidence spectroscopy
Magnetic-bottle electron spectrometer

ABSTRACT

Multi-electron coincidence spectroscopy using a magnetic-bottle electron spectrometer has been applied to the study of the Auger decay following O1s photoionization of condensed H_2O molecules. Coincidence Auger spectra are obtained for three different photoelectron energy ranges. In addition, the energy distribution of the slow electrons ejected in the Auger decay of the O1s core hole is deduced from three-fold coincidences.

1. Introduction

Absorption of a single high-energy photon by a condensed matter often results in emissions of two or more electrons from the surface. Auger decay following inner-shell photoionization of the constituents of the condensed matter is one of the important origins of the multi-electron emissions, while the emissions of multiple valence-band electrons also occur sizably as a result of multi-electron photoemission and inelastic scattering of initially-ejected electron [1]. Electron coincidence spectroscopy, which enables one to clarify energy correlations between electrons emitted in pair, is especially useful to identify the individual pathways of the multi-electron emission processes [2,3]. In order to obtain reasonable coincidence efficiencies, electron spectrometers with large acceptance solid angles have been adapted to the electron coincidence measurements. For example, Thurgate and co-workers have improved photoelectron-Auger electron coincidence apparatuses based on two hemispherical analyzers [4], and Mase and co-workers have developed a coincidence apparatus consisting of a symmetric mirror analyzer and a cylindrical mirror analyzer [5]. Kirschner and co-workers have utilized two hemispherical energy analyzers installed with two-dimensional detectors [6,7]. Meanwhile, Gotter et al. have demonstrated angle-resolved photoelectron-Auger electron coincidence measurements using an array of seven hemispherical spectrometers [8]. However, statistics and energy resolution of coincidence spectra have been occasionally compromised even in such two-electron coincidence measurements.

In this work, we have introduced for the first time the magnetic bottle technique [9] into electron coincidence investigation of multi-electron emissions from solid surfaces. This technique, enabling one to collect almost all the electrons emitted into the whole solid angle, has been successfully used in electron coincidence studies for gas-phase atoms and molecules. Thanks to the extremely-high collection-efficiency, not only two-electron coincidence but also multi-electron coincidences (three-fold or more) have been effectively achieved, and varieties of multi-electron emission pathways including such topical processes as triple photoionization [10,11] and double core photoionization [12] have been disclosed. In the present study, the feasibility of a magnetic-bottle electron spectrometer for solid samples is demonstrated by its application to multi-electron emissions from water molecules condensed thickly on solid surface.

Electron emission processes from water molecules are of particular interest, because of their connection with radiation damage of bio-cells. The DNA strand breaks in bio-cells exposed to ionizing radiations are caused partly by the impacts of electrons emitted from the ionization of cell-solvent water, where the impact of

* Corresponding author.
E-mail address: hikosaka@las.u-toyama.ac.jp (Y. Hikosaka).

http://dx.doi.org/10.1016/j.elspec.2016.10.006
0368-2048/

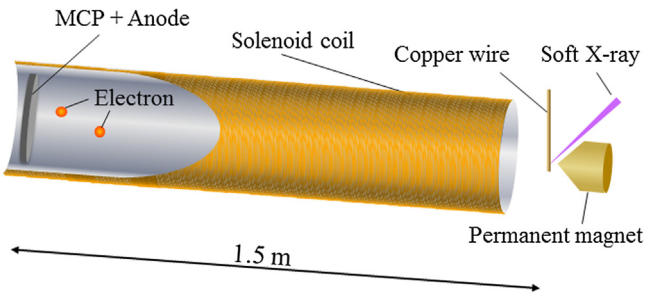

Fig. 1. Schematic of the magnetic bottle electron spectrometer.

slow electrons can efficiently induce DNA strand breaks through resonant capture processes [13,14]. An important fraction of the slow electrons can be produced in the Auger decay of the core-hole formed by the initial inner-shell ionization. For isolated water molecules, the slow electron formation relevant to the inner-shell photoionization has been investigated by multi-electron coincidence spectroscopy [15]. It was observed that the autoionizing O atoms produced by the dissociation of Auger-final H_2O^{2+} states remarkably yield discrete structures in the energy distribution of the slow electrons [15]. It is interesting to investigate whether the energy distribution of the slow electrons from solvent water condensed by hydrogen bonding also shows such discrete structures.

In this study, we have investigated multi-electron emissions from condensed water molecules and obtained coincidence Auger spectra with satisfactory statistics. Moreover, the energy distribution of the slow electrons ejected in the Auger decay of the O1s core hole is deduced from three-fold coincidences, where any tangible structure due to O autoionization cannot be identified. To our knowledge, such a three-fold coincidence has never been achieved for solid samples, which verifies the powerfulness of the magnetic bottle technique in electron coincidence spectroscopy for multi-electrons ejected from surfaces.

2. Experimental

The experiment was performed at the beamline BL4B of the synchrotron radiation facility UVSOR. The single bunch operation of the storage ring provided light pulses with a 178-ns repetition period for the 110-ps-width light-pulses. The synchrotron radiation from a bending magnet of the storage ring was monochromatized by a grazing incidence monochromator using a varied-line-spacing plane grating. The monochromatized light was focused to 0.5 mm (horizontal) × 0.3 mm (vertical) in size.

Electron coincidence measurements were carried out with the magnetic bottle electron spectrometer [16] whose schematic is shown in Fig. 1. A strong permanent magnet whose top is of a conical shape (~1 T at the tip) is placed a few mm away from the focal point of the monochromatized light. A 1.5-m long solenoid tube, forming a homogeneous magnetic field (~1 mT) in its inside, faces to the permanent magnet across the focal point of the monochromatized light. Electrons formed around the focal point are captured by the magnetic field lines and are guided towards the microchannel plate detector located around the opposite end of the solenoid tube. Signals from the detector are fed into a multi-stop time-to-digital converter (Roentdek TDC8). Conversion from the electron time-of-flight to kinetic energy was calibrated by measuring Ar 2p photoelectron spectra at many different photon energies. The energy resolving power of the apparatus was estimated, from the photoelectron lines, to be nearly constant at $E/\Delta E = 35$ [16]. It was also estimated from the coincidence yields between Ar 2p photoelectrons and the corresponding Auger electrons that the electron

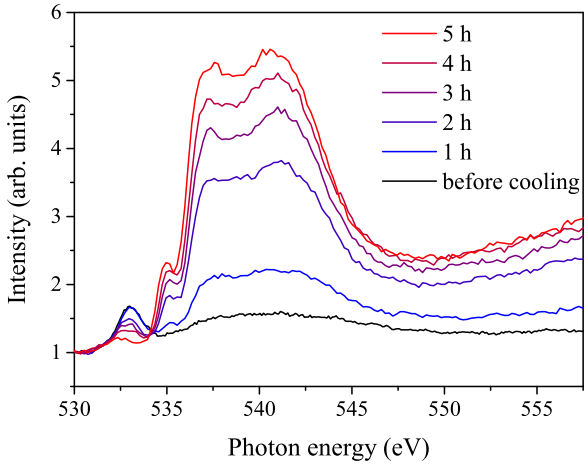

Fig. 2. Total electron yield spectra around oxygen K-edge, measured before and under the cooldown (cooling time of 1–5 h) of the copper wire. The photon energy resolution is around $E/\Delta E = 5000$. Intensities of the spectra were normalized at 530 eV.

detection efficiencies decrease slowly with electron kinetic energy from ~50% (E ≈ 0 eV) to ~40% (E = 600 eV) [16].

In the present measurement, a copper wire of a 0.3-mm diameter was placed at the focus point of the monochromatized light, at right angles to the photon beam and the solenoid tube axis. No particular cleaning was applied to the wire surface, and hence it should be severely contaminated with carbon and oxygen. Water molecules were adsorbed on the surface by continuously cooling the wire down to the liquid nitrogen temperature, under exposure to the background pressure inside the chamber ($\sim 1.8 \times 10^{-8}$ Torr) in which water vapor should be one of the dominant residual gases. In practice, the background pressure decreased to $\sim 1.0 \times 10^{-8}$ Torr during cooling, according to the condensation of water vapor.

Fig. 2 shows total electron yield spectra around oxygen K-edge, measured before and under cooling of the copper wire. Through the present work, both the entrance and exit slits of the monochromator were set to be extremely narrow in order to reduce the electron count rate to less than 10 kHz, and the photon energy resolution reached the best value ($E/\Delta E = 5000$) of the monochromator. As seen in Fig. 2, before the cooldown of the copper wire, the total electron yield spectrum shows a single peak around 533 eV. As cooling time goes on, while the peak around 533 eV becomes weaker and shifts lower photon energy side, an enhancement appeared in 535–545 eV remarkably grows up. The spectrum after 2-h cooling, which exhibits a broad band with maxima around 537 V and 542 eV and a weak shoulder around 535 eV, resembles closely the NEXAFS spectra of ice [17–19], certifying thick adsorption of water molecules on the wire surface. The spectral intensity increases with increasing cooling time of more than 2 h, implying that the thickness of the condensed water layer is still comparable to the escape depths of the ejected electrons (~1 nm for 500 eV electrons [20]). This is because, considering that electrons generated at a distant depth much beyond their escape depth can hardly get out into the vacuum, further growth of the layer whose thickness already got much beyond the escape depth does not results in such an increase of the electron yields.

3. Results and discussion

Coincidence datasets were accumulated for electrons emitted from the copper wire on irradiation of 738.2 eV photons, before and under the cooldown. The measurement under the cooldown was started after an advance cooling of 2 h, to ensure sizable adsorption of water molecules on the wire surface. The photon energy

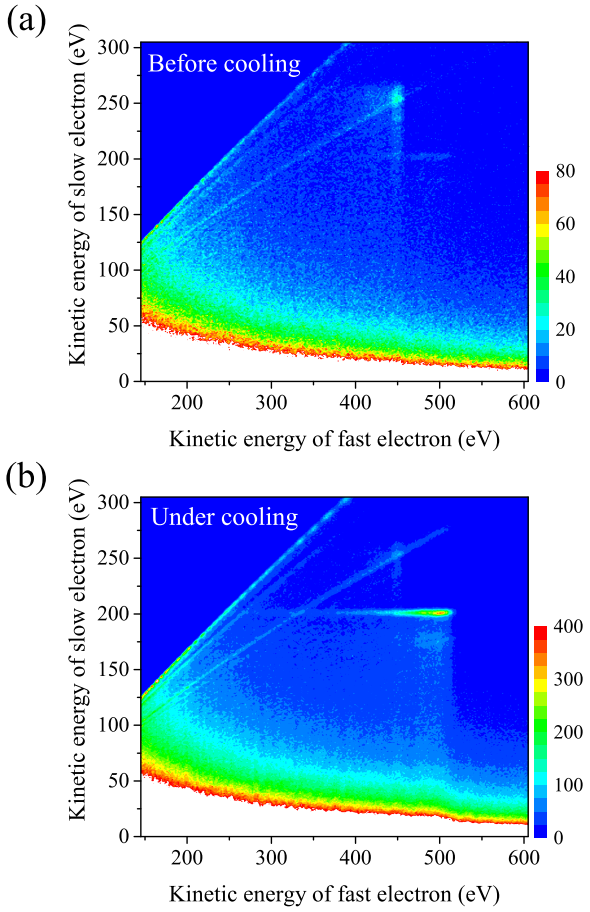

Fig. 3. Two-dimensional maps showing energy correlations of the coincident electrons emitted from the copper wire on irradiation of 738.2 eV photons, (a) before and (b) under the cooldown to the liquid nitrogen temperature. The measurement under the cooldown was started after an advance cooling of 2 h, to ensure a thick adsorption of water molecules on the wire surface. The accumulation times were 3 h and 20 h, respectively, with count rates around 5 kHz.

is ~200 eV above the O1s threshold of condensed water (~533 eV [17,21]). The two-dimensional maps in Fig. 3 display the energy correlations of the coincident electrons included in the accumulated coincidence datasets, where the coincidence counts are plotted as a function of faster (x-axis) and slower electron energies (y-axis). Several diagonal lines seen commonly in these two maps are artifacts due to rebounds in the electron signals. On the map from the accumulation before the cooldown [Fig. 3(a)], a weak structure running vertically is discernible around (x, y) = (450 eV, 230–260 eV). This structure is ascribable to the coincidences between the C1 s photoelectrons (450 eV) and the C1 s Auger electrons (230–260 eV) ejected from the carbon contamination on the wire. The corresponding structure becomes less remarkable in the map from the accumulation under the cooldown [Fig. 3(b)], but otherwise a clear structure running horizontally appears around (x, y) = (400–530 eV, 200 eV). The emergent structure is assignable to the coincidences between the O1s photoelectrons (200 eV) and the O1s Auger electrons (400–530 eV) from condensed water molecules.

To display the O1s photoelectron structure closely, the coincidence counts on the map in Fig. 3(b) are integrated in the range of x = 450–530 eV and projected onto y-axis. The spectrum thus obtained is presented in Fig. 4. The O1s photoelectron peak is observed around a kinetic energy of 205 eV, and a continuous structure is remarkably exhibited on the lower kinetic energy side. The continuous structure is attributed mainly to the photoelectrons with reduced energies due to inelastic scatterings on

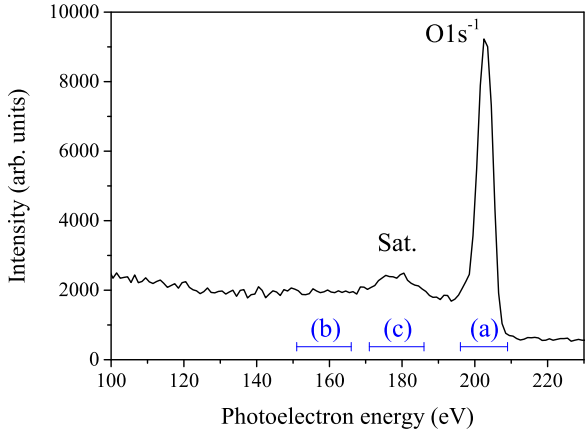

Fig. 4. Photoelectron spectrum obtained by integrating the coincidence counts on the map in Fig. 3(b) over the range of x = 450–530 eV. The three kinetic energy ranges for the extractions of the curves in Figs. 5(a)-(c) are indicated.

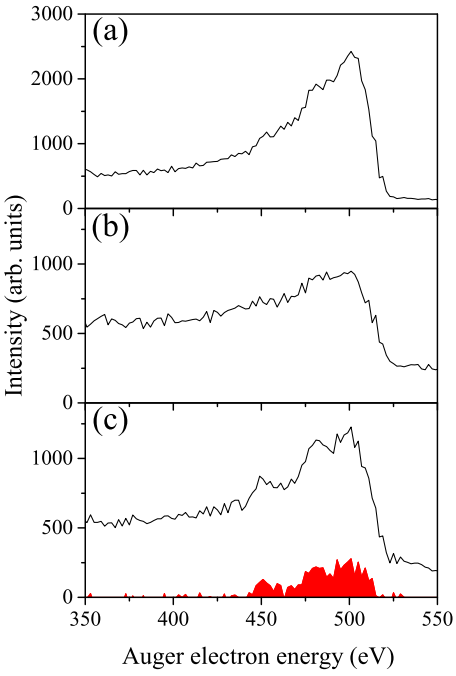

Fig. 5. Auger electron spectra obtained in coincidence with (a) O1s photoelectrons, (b) energy-loss photoelectrons due to inelastic scatterings, and (c) electrons in the broad maximum. The photoelectron energy ranges set for the extractions of these Auger spectra are indicated in Fig. 4. In (c), the raw Auger spectrum (solid black) includes a large contribution from the inelastic scattering process, and net spectrum (red filled area) is obtained by assuming that the contribution from the inelastic scattering is described by the distribution in (b). (For interpretation of the references to colour in this figure legend, the reader is referred to the web version of this article.)

the escape from the inside of the water condensation. On the continuum structure, a broad maximum is discernible around a kinetic energy of 180 eV. One may consider that this structure is due to an enhancement in the inelastic scattering at the specific energy loss corresponding to the valence excitation in the counterpart water molecules. In the meanwhile, for monolayer H_2O adsorbed on Si surface, the formation of 1 s satellite states resulting from the promotion of a valence electron accompanying O1s ionization is observed with a similar energy separation [22]; this single-molecule process possibly contributes to the enhancement observed for the present multi-layer sample.

Fig. 5 presents Auger electron spectra observed in coincidence with O1s photoelectrons (region (a) in Fig. 4), energy-loss

photoelectrons due to inelastic scatterings (region (b) in Fig. 4), and electrons in the broad maximum (region (c) in Fig. 4). The Auger spectrum in coincidence with O1s photoelectrons, shown in Fig. 5(a), resembles the conventional Auger spectrum [23]. Considerable intensity is observed even below 420 eV, which is ascribable to an energy loss of the Auger electrons due to the inelastic scattering. In the Auger spectrum derived in coincidence with energy-loss photoelectrons due to inelastic scatterings [Fig. 5(b)], the O1s Auger feature is less pronounced compared to that in Fig. 5(a), implying that effect from inelastic scattering is enhanced in the selection to the low energy tail of the O1s photoelectron peak. This observation can be understood as follows: the selection of photoelectrons with energy loss picks out the photoemission events for H_2O molecules distant from the outermost surface and thus the Auger electrons ejected from these molecules are also subject to remarkable inelastic scattering.

The raw coincidence Auger spectrum deduced for the broad maximum [solid black curve in Fig. 5(c)] includes a large contribution from the ordinary inelastic scattering process, corresponding to the background intensity underling the enhancement structure seen in Fig. 4. Assuming that the spectral shape of the contribution from the ordinary inelastic scattering process is rarely dependent on the kinetic energy of the energy-loss photoelectron and is described by the spectrum in Fig. 5(b), the contribution can be reasonably subtracted from the raw spectrum. The residual spectrum, shown as red filled area in Fig. 5(c), exhibits an Auger structure in which low kinetic energy tail due to the inelastic scattering is less remarkable. Thus, it is likely that the main contributor to the enhancement is the formation of the 1 s satellite states. The Auger structure in the red filled area in Fig. 5(c) lies in a similar energy range to the Auger decay of the O1s state [Fig. 5(a)], though the 1 s satellite states gain an excess energy of the valence excitation compared to the main O1s state. A similar behavior is observed in the Auger decay of the O1s satellite states in isolated H_2O molecules [15]. These observations are understood in terms of the spectator behavior of the excited valence electron: the excited valence electron is kept in the initially-excited orbital through the Auger decay and the Auger final states are correspondingly more excited.

Since O1s photoionization of a single H_2O molecule is predominantly followed by the Auger decay, the O1s photoelectron and Auger electron are basically emitted in pair from the molecule. However, a considerable fraction of these electrons should be lost in the way to the ejections into the vacuum. In practice, in the coincidence dataset accumulated under the cooldown, coincidence count between O1s photoelectron and O1s Auger electron is 4.5% of the total count of the O1s photoelectron and 1.4% of that of the Auger electron, where the Auger electrons in the kinetic energy range of 450–530 eV are chosen. Here, the total count of the Auger electron was observed to be three times as much as that of the photoelectron. The higher ejection probability for the Auger electrons is a good correspondence to the fact that the electron escape depth for the Auger electrons (kinetic energy ~500 eV) is a few times larger than that for the O 1 s photoelectron (kinetic energy ~200 eV) [20].

Next, we inspect the slow electron emission accompanying the Auger decay of the O1s core hole. Such slow electrons should be observed in three-fold coincidence with the O1s photoelectron and the fast Auger electron. Fig. 6 displays the energy correlation between the photoelectrons (x-axis) and additional slow electrons (y-axis) in the kinetic energy range of 0–6 eV, obtained from the triple coincidence events including a fast Auger electron in the kinetic energy range of 450–530 eV. A vertical stripe is seen at the O1s photoelectron energy, delineating the distribution of the slow electrons accompanying the Auger decay of the O1s core hole. The slow electron spectrum extracted by the yields along the vertical stripe is shown in the right panel. The slow electron spectrum shows a continuous distribution decreasing gradually as increasing the electron energy. It is reported for isolated H_2O molecules that a similar continuous distribution of slow electrons is produced through the double Auger decay of the O1s core-hole state [15]; it is likely, however, that the contribution from the double Auger decay is minor in the slow electrons ejected from condensed water. This is because, while the sum of the energies of the two Auger electrons emitted in the double Auger process should show the H_2O^{3+} states populated finally, the corresponding H_2O^{3+} structures cannot be identified in the sum of the energies of the fast Auger electron and slow electron (not shown). Therefore, majority of the slow electrons observed in the O1s decay of the condensed water is probably the secondary electrons produced by scatterings of the ejecting photoelectrons and Auger electrons.

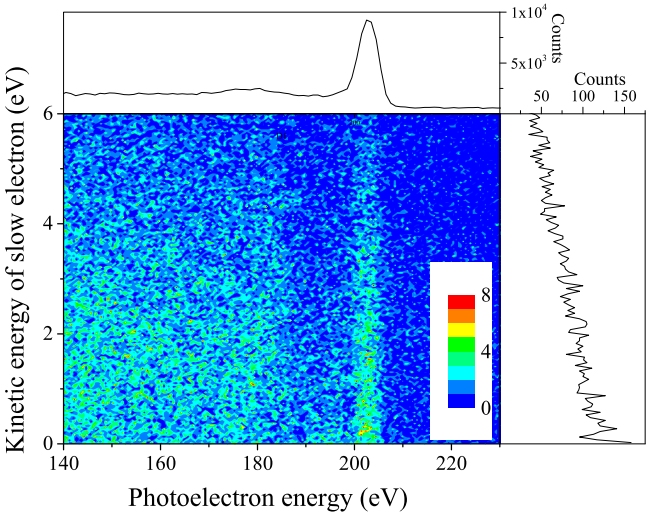

Fig. 6. Two-dimensional map showing energy correlation between the O1s photoelectrons and slow electron below a kinetic energy range of 6 eV, which is extracted from the triple coincidence events including a fast Auger electron in the kinetic energy range of 450–530 eV. The top panel shows an enlargement of the spectrum in Fig. 4, and the right panel plots the slow electron spectrum extracted by integrating the horizontal range for the O1s photoelectrons.

The total counts of the spectrum in the right panel in Fig. 6, corresponding to the yields of the three-fold coincidences among the O1s photoelectron, the fast Auger electron and the slow electron, are about 17% of the number of the coincidences between the O1s photoelectron and the fast Auger electron. By taking the detection efficiency (~50%) of the slow electron into account, ~34% of the pairs of the O1s photoelectron and fast Auger electron are accompanied by the ejection of a slow electron in the range of 0–6 eV. This observation implies that slow electrons are efficiently formed by the inelastic scattering of photoelectrons and Auger electrons. Note that, considering that the escape depth [20] for the slow electrons less than 6 eV is an order of magnitude larger than that of the fast Auger electron, the ejection probability for the slow electrons should be significantly large.

The distribution of the slow electrons emitted after O1s photoionization in isolated H_2O molecules remarkably exhibits below 2 eV the autoionization lines of superexcited O atoms [15]. These superexcited O atoms are formed by double OH-bond breaking at highly-excited H_2O^{2+} states populated after the Auger decay of the O1s core-hole state. The corresponding autoionization lines are hardly discernible in the slow electron distribution in the right panel of Fig. 6. Since the superexcited O formation constitutes only 0.8% in the O1s decay of the isolated H_2O molecules [15], even if this process occurs similarly in condensed phase, the autoionization lines are masked by the slow electrons formed efficiently by the inelastic scattering. On the other hand, it is anticipated that the formation of superexcited O atoms is suppressed in condensed

phase, because of fast electron transfers from neighbor molecules to the Auger final states before their dissociation.

In conclusion, we have applied multi-electron coincidence spectroscopy using a magnetic bottle electron spectrometer to multi-electron emissions from condensed water molecules. Coincidence Auger spectra were obtained not only for the O1s decay but also for the satellite decay. Moreover, three-fold electron coincidence was achieved. The present work demonstrates that the magnetic bottle technique is promising in electron coincidence measurements of solid samples.

Acknowledgments

The authors thank Kazuhiko Mase (KEK-PF) for fruitful discussions. We are grateful to the UVSOR staff for the stable operation of the storage ring. This work was supported by the Cooperative Research Program of the Institute for Molecular Science. YH thanks financial supports from Shimadzu Science Foundation and Daiko Foundation.

References

[1] S. Satyal, P.V. Joglekar, K. Shastry, S. Kalaskar, Q. Dong, S.L. Hulbert, R.A. Bartynski, A.H. Weiss, J. Electron Spectrosc. Relat. Phenom. 195 (2014) 66.
[2] H.W. Biester, M.J. Besnard, G. Dujardin, L. Hellner, E.E. Koch, Phys. Rev. Lett. 59 (1987) 1277.
[3] G. Stefani, R. Gotter, A. Ruocco, F. Offi, F. Da Pieve, S. Iacobucci, A. Morgante, A. Verdini, A. Liscio, H. Yao, R.A. Bartynski, J. Electron Spectrosc. Relat. Phenom. 141 (2004) 149.
[4] G.A. van Riessen, S.M. Thurgate, Surf. Interface Anal. 38 (2006) 691.
[5] T. Kakiuchi, E. Kobayashi, N. Okada, K. Oyamada, M. Okusawa, K.K. Okudaira, K. Mase, J. Electron Spectrosc. Relat. Phenom. 161 (2007) 164.
[6] G. van Riessen, Z. Wei, R.S. Dhaka, C. Winkler, F.O. Schumann, Jürgen Kirschner, J. Phys.: Condens. Matter 22 (2010) 092201.
[7] Z. Wei, F.O. Schumann, C.H. Li, L. Behnke, G. Di Filippo, G. Stefani, J. Kirschner, Phys. Rev. Lett. 113 (2014) 267603.
[8] R. Gotter, A. Ruocco, A. Morgante, D. Cvetko, L. Floreanoa, F. Tommasini, G. Stefani, Nucl. Inst. Meth. Phys. Reas. A 467-468 (2001) 1468.
[9] J.H.D. Eland, O. Vieuxmaire, T. Kinugawa, P. Lablanquie, R.I. Hall, F. Penent, Phys. Rev. Lett. 90 (2003) 053003.
[10] Y. Hikosaka, P. Lablanquie, F. Penent, T. Kaneyasu, E. Shigemasa, R. Feifel, J.H.D. Eland, K. Ito, Phys. Rev. Lett. 102 (2009) 013002.
[11] Y. Hikosaka, P. Lablanquie, F. Penent, J. Palaudoux, L. Andric, G. Gamblin, K. Soejima, E. Shigemasa, M.I.H. Suzuki, Nakano, K. Ito, Phys. Rev. Lett. 107 (2011) 1130052.
[12] P. Lablanquie, F. Penent, Y. Hikosaka, J. Phys. B 49 (2016) 182002.
[13] B.D. Michael, P.A. O'Neill, Science 287 (2000) 1603.
[14] B. Boudaïffa, P. Cloutier, D. Hunting, M.A. Huels, L. Sanche, Science 287 (2000) 1658.
[15] Y. Hikosaka, K. Yamamoto, M. Nakano, T. Odagiri, K. Soejima, I.H. Suzuki, P. Lablanquie, F. Penent, K. Ito, J. Chem. Phys. 137 (2012) 191101.
[16] Y. Hikosaka, M. Sawa, K. Soejima, E. Shigemasa, J. Electron Spectrosc. Relat. Phenom. 192 (2014) 69.
[17] A. Křepelová, J. Newberg, T. Huthwelker, H. Bluhm, M. Ammann, Phys. Chem. Chem. Phys. 12 (2010) 8870.
[18] Ph. Parent, C. Laffon, C. Mangeney, F. Bournel, M. Tronc, J. Chem. Phys. 117 (2002) 10842.
[19] S. Myneni, Y. Luo, L.Å. Näslund, L. Ojamäe, H. Ogasawara, A. Pelmenschikov, P. Väterlein, C. Heske, L.G.M. Pettersson, A. Nilsson, J. Phys. Condens. Matt. 14 (2002) L213.
[20] M. De Crescenzi, M.N. Piancastelli, Electron Scatt. Relat. Spectrosc. World Sci. (1996).
[21] S. Yamamoto, H. Bluhm, K. Andersson, G. Ketteler, H. Ogasawara, M. Salmeron, A. Nilsson, J. Phys.: Condens. Mater. 20 (2008) 184025.
[22] S. Tanaka, K. Mase, S. Nagaoka, M. Nagasono, M. Kamada, J. Chem. Phys. 117 (2002) 4479.
[23] K. Mase, M. Nagasono, S. Tanaka, T. Urisu, E. Ikenaga, T. Sekitani, K. Tanaka, Surf. Sci. 390 (1997) 97.